ISSN 2580-0817

Computational Fluid Dynamics Analysis of Temperature Distribution in Solar Distillation Panel with Various Flat Plate Materials

Trismawati[1], Hendry Y. Nanlohy[2*], Helen Riupassa[2], Susi Marianingsih[3]

[1]*Department of Industrial Engineering, Panca Marga University, Probolinggo, 67271, Indonesia*
[2]*Department of Mechanical Engineering, Jayapura University of Science and Technology, 99351, Indonesia*
[3]*Faculty of Computer Science and Management, Jayapura University of Science and Technology, 99351, Indonesia*
**Corresponding author: hynanlohy@gmail.com*

Article history:
Received: 19 May 2024 / Received in revised form: 29 June 2024 / Accepted: 3 July 2024
Available online 7 July 2024

ABSTRACT

As the world population continues to grow, the demand for clean water is increasing daily, making it a crucial resource to access. However, there are ways to harness abundant resources like solar energy and seawater to produce clean water. The present studies have conducted experimental investigations to convert seawater into freshwater using solar stills, where solar energy is utilized as the primary heat source for evaporation. The temperature distribution inside the solar stills was analyzed using a flat plate made of three different materials: copper, stainless steel, and aluminum. To examine the temperature distribution and performance of the solar stills, researchers employed computational fluid dynamics simulations (Ansys R15.0). The results showed variations in temperature distribution among the three plate materials. Copper flat plates achieved the highest temperature, approximately 44.5 Celsius, followed by aluminum at 43.91 Celsius, while stainless steel exhibited the lowest temperature at around 42.01 Celsius. The average heat flux across the three materials was approximately 581 W/m^2. Additionally, observations indicated that the amount of convection occurring in copper flat plates was 121.108 Watts; in aluminum, it was 118.517 Watts; and in stainless steel, it was 105.05 Watts. The radiation energy for stainless steel flat plates was 29.93 W; for copper, 16.14 W; and for aluminum, 13.49 W.

Keywords: *CFD analysis, seawater desalination, solar energy, temperature distribution phenomena, various materials*

I. Introduction

Renewable energy has witnessed a significant surge in most parts of the world in recent years due to its numerous benefits [1]-[3]. Renewable energy can generate a range of necessities such as electricity, hot water, fresh water, fuels, catalysts, additives, and more [4]-[6]. While some renewable sources like wind turbines and sea waves only generate electricity, solar energy is an incredibly versatile source that can be employed for various purposes such as generating electricity, hot water, hot air, cooking, and drying [7], [8]. However, solar energy, in particular, is an essential renewable source that can produce electricity, hot water, and even drinking water [9]. Solar power is harnessed by using solar panels that convert sunlight into electricity. Solar water heaters use the sun's energy to heat water, and the heated water can be utilized for various purposes, including showering, cooking, and cleaning [10], [11]. Solar air heaters use the sun's energy to heat air, which can be used to warm up indoor spaces [12]. Solar cookers are also

DOI:10.17977/um0168i12024p108

becoming increasingly popular, as they can cook food without gas or electricity.

In areas with high solar intensity but lacking fossil fuels, solar water desalination can be a viable option to meet daily water needs. Solar water desalination is a process that involves using solar energy to purify seawater and make it drinkable [13], [14]. This process is beneficial in regions where fresh water is scarce and people must rely on seawater for daily needs [15]. Sunlight and seawater are two abundant alternative energy sources that have great potential to produce clean and healthy water. Solar energy has been identified as the primary heat source for seawater desalination technology, which can produce high freshwater yields at a low cost [16], [17]. The current distillation and water purification equipment in the market are complex and expensive, making them inaccessible to people living inland. Previous studies have developed a natural convection process that utilizes solar radiation, also known as passive solar stills, to overcome this [18]-[20]. However, these passive solar stills have low productivity levels [21]. They have employed various methods such as nanotechnology, thermoelectric coolers, glass cooling, phase change material, solar collectors, and auxiliary condensers to enhance their efficiency [22], [23]. These methods can increase thermal efficiency, freshwater generation, and water productivity, but they require additional equipment that increases energy consumption and cost, making them inefficient [19], [24].

Our research aims to study the comparative performances of solar stills with three different materials: copper, stainless steel, and aluminum. These three materials are selected based on prior research highlighting copper's exceptional thermal conductivity, which facilitates highly efficient heat transfer. Additionally, copper boasts good corrosion resistance, making it well-suited for demanding environments [25]. However, the elevated cost of copper can escalate the expenses associated with the fabrication and installation of solar water heating systems [26]. On the other hand, stainless steel is a sturdy and corrosion-resistant material. Despite its lower thermal conductivity compared to copper, stainless steel offers merits in terms of mechanical strength and longevity. Its use can balance cost, durability, and thermal efficiency [25].

Meanwhile, aluminum presents a distinctive combination of commendable thermal conductivity, lightweight properties, and relatively low cost [27]. Furthermore, aluminum exhibits good corrosion resistance, particularly when coated with protective materials such as anodizing [28]. Its lightweight nature facilitates easier installation and imposes less strain on supporting structures. Nonetheless, it requires additional treatment to enhance its corrosion resistance to a level comparable to copper and stainless steel [29].

Several recent studies have utilized Ansys computational fluid dynamics CFD for solar desalination. For instance, Jawed et al. [30] employed Ansys Fluent to optimize the geometric design of solar collectors in a desalination system. Through testing various geometric configurations, they identified that a parabolic collector with a specific inclination angle can enhance heat absorption efficiency by up to 18% compared to a conventional flat design. Furthermore, Abolfazl et al. [31] used Ansys Fluent to model the thermohydraulic process in a multi-effect solar desalination system, focusing on how fluid flow and temperature distribution variations affect desalination efficiency. They found that adjusting the flow rate settings can increase freshwater production by up to 22% by mitigating efficiency losses caused by hot spots.

Additionally, studies by Masoud et al. [32] and Patrick et al. [33] modeled the solar stills system to enhance their efficiency. It was concluded that by optimizing the design of the

evaporation chamber and condensation surface, the evaporation and condensation efficiency could be increased by up to 25%. Wind speed was also found to impact the condensation rate and overall system efficiency, as high wind speeds can increase the condensation rate but also lead to significant heat loss. Unfortunately, previous studies only focused on the active solar stills method. Therefore, this present research proposes the complete passive solar stills method and CFD analysis to determine flow patterns, condensing cover and adjacent walls behavior, evaporation zone, condensing zone, and moisture zone. Moreover, thermal efficiency in a solar still simulation can be achieved by changing geometric and physical parameters such as cooling water velocity, film cooling thickness, and water glass cooling thermal characteristics.

Unlike the performance parameters mentioned above, CFD analysis is used to determine the temperature and heat flux distribution of the three materials used in this research. Our study provides valuable insights into the comparative performances of solar stills with different materials and helps identify the most efficient and cost-effective method for producing clean and healthy water.

II. Material and Methods

The data collection and analysis in this study required various equipment, including a laptop, a K-type thermocouple, a solar power meter, and an HHTEC distillery refractometer. The experimental apparatus and process, including data collection, can be seen in Figure 1. To act as an insulator, the study opted for rock wool, a mineral fiber that is inexpensive and renowned for its fire protection and acoustic and thermal properties. The geometry of a solar distillation panel is as follows. Length of base panel (L) = 1m; Width (W) = 1m; Angle of inclination (θ) = 30°; Depth of water Basin (d) = 0.1m; Length of Inclined cover (L) = 1.154m (for $\theta = 30°$). Schematically, the research installation can be seen in Figure 2.

Harnessing solar energy for seawater distillation was the primary focus of the study, and the study discovered that the thermal conductivity average was roughly 0.034 W/m.ºC, which was measured between 100ºC and 820ºC. This information is vital for developing more sustainable and efficient seawater distillation methods, which could positively affect the environment and assist in addressing the global water crisis [34].

The data collection process involved several stages, which are listed below in detail [35]:

1. Preparation of tools and materials included a solarimeter to measure solar intensity. In addition, a refractometer to measure the salt content in seawater, a device to measure the dimensions of the absorption plates in solar distillation, and other necessary equipment should be prepared. Measuring and recording the salt content in seawater using a refractometer: The salt content in seawater was measured using a refractometer, an instrument used to measure the index of refraction of a liquid. The readings were recorded for future use.
2. Measuring and recording the dimensions of the absorption plates in solar distillation: The dimensions of the absorption plates in solar distillation were measured and recorded. This information was necessary to calculate the surface area of the plates and to determine the efficiency of the solar distillation process.

3. Conducting solar distillation from 09:00 am to 04:00 pm, with data collected every hour: The solar distillation process was conducted for seven hours, and during this time, data was collected every hour to monitor the efficiency of the process.
4. Recording various temperatures during distillation: These included ambient temperature, glass temperature, plate temperature, water vapor temperature in the distillation, and water temperature in the distillation. The overall test results are presented in Tables 1, 2, and 3.
5. Recording the volume of water: This included the incoming water volume, produced water volume, and residual water volume.
6. Processing the collected data: The collected data was processed per the simulation requirements. This involved test equipment schemes, modeling, and meshing depicted in Figure 3, 4, and 5. The processed data was then used for further analysis and research.
7. The boundary conditions for this experiment are as follows: a heat flux of 640 W/m², convection to the surrounding air with a heat transfer coefficient of 10 W/m^{2}K, and an ambient temperature of 30°C. The initial temperature of all materials on the panel is 30°C.

Fig. 1. Experimental process and data collection

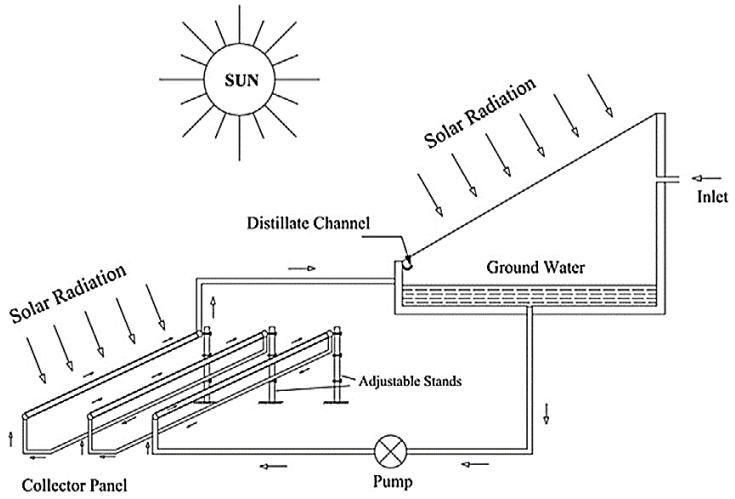

Fig. 2. Experimental scheme

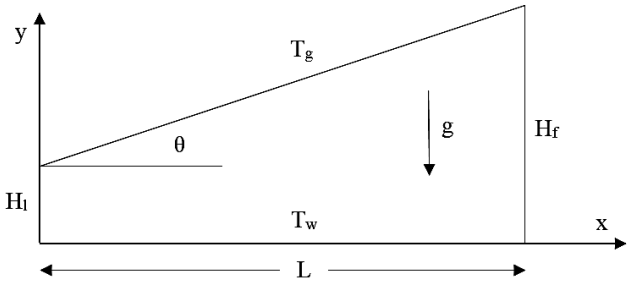

Fig. 3. The schematic view of the solar still

Meanwhile, capturing the interface between water and steam during distillation requires using the Volume of Fluid (VOF) method. This method is effective for modeling two-phase flows with clear interfaces with the following steps:

1. Geometry and mesh preparation: Create or import the model geometry in Ansys type/edition or Space Claim. Mesh the model using Ansys meshing. Make sure the mesh is fine enough near the water and steam interface to capture the interface details well.
2. Physical model settings: Model: Activate the volume of fluid (VOF) model in Ansys Fluent; Phase: Define two phases: water and steam (or water and air, depending on the case); Material Properties: Define the material properties of each phase (density, viscosity, etc.)
3. Boundary conditions: Define the boundary conditions for the inlet, outlet, and walls according to operating conditions. The inlet condition is usually water or steam; the outlet is where the gas or liquid phase exits.
4. Initial conditions: Define the initial conditions for the phase distribution (e.g., water at the bottom and air at the top). Use the initialization function to define the initial distribution of the phases.
5. Heat transfer and transport model: Activate the heat transfer model if necessary and define the thermal conditions at the walls and interfaces.
6. Solver settings: According to the problem, select a pressure-based or density-based solver. Enable a suitable discrimination scheme, such as the Geo-Reconstruct scheme for phase interfaces, for good stability and convergence.
7. Simulation and monitoring: Run simulations and monitor the convergence of key parameters such as velocity, pressure, and phase volume fractions. Visualize the water/vapor interface using post-processing in Ansys Fluent or CFD-Post.

Meanwhile, to model radiation transport through glass using the discrete ordinates (DO) method, the steps are the same as those for the volume of fluid (VOF) method when capturing the water interface during distillation. The flowchart of the typical numerical modeling can be seen in Figure 6.

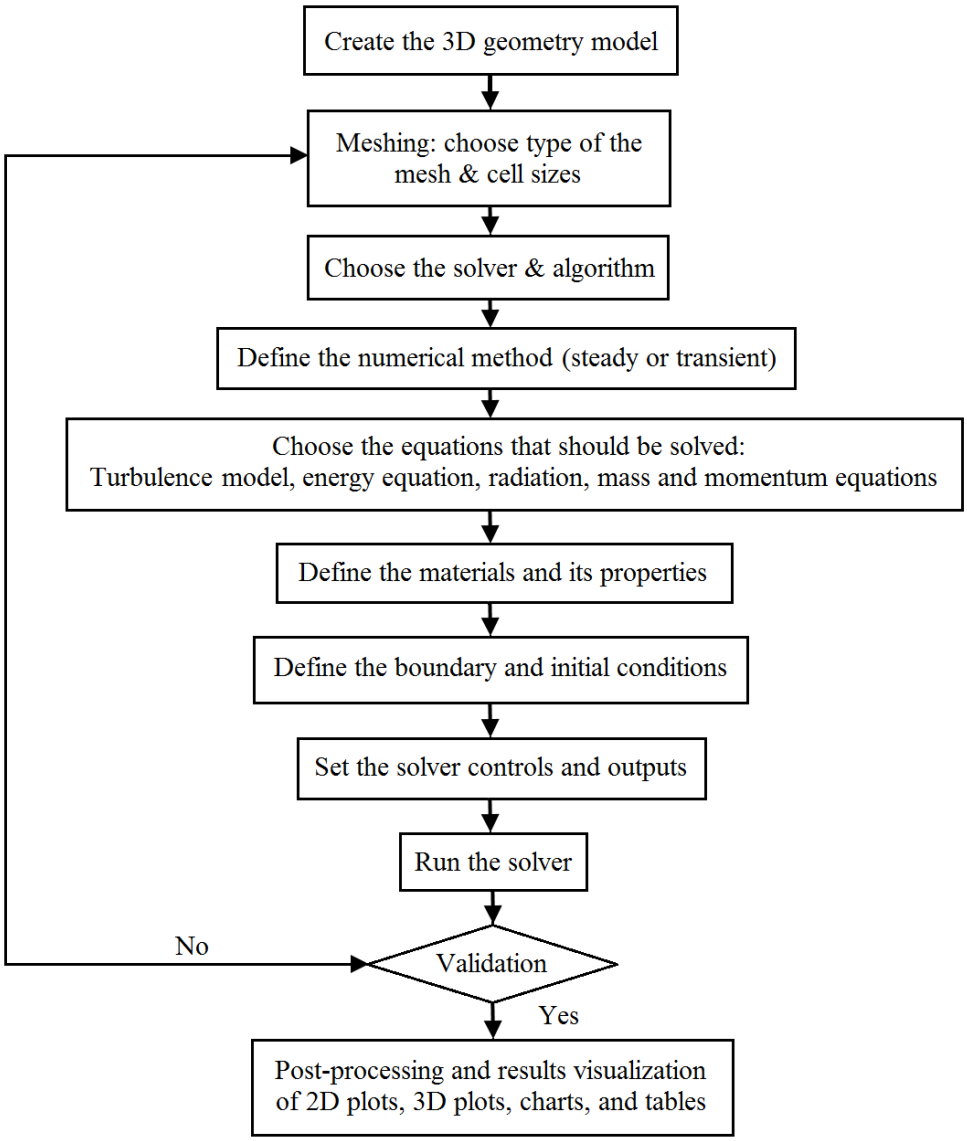

Fig. 4. Flowchart of the typical numerical modeling

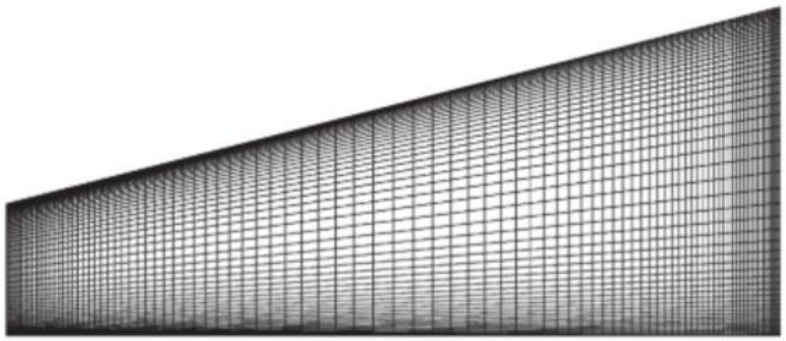

Fig. 5. The mesh distribution of solar panel distillation

III. Result and Discussion

Tables 1 to 3 and Figure 6 present the comprehensive results obtained from the performance testing of solar panels composed of various materials i.e. copper, stainless steel, and aluminum. One notable aspect of the testing is that the environmental temperature for all three materials ranges between 31 and 35°C. Furthermore, the temperature varies throughout the day, with the lowest temperatures recorded in the morning and afternoon, while the highest temperatures are typically observed between 12.00 and 02.00 p.m. The degree of absorption of sunlight intensity serves as an indicator of solar panel performance. Notably, the testing results revealed that the highest absorption intensity was recorded for aluminum materials, at 656.23 W/m^2, followed by stainless steel at approximately 562.58 W/m^2, and copper at 526.28 W/m^2.

Table 1. Experimental result for copper

Time (hr)	Temperature (^{o}C)				Water (Liter)				Solar intensity (W/m^2)
	Environment (Tl)	Plate (Tp)	Glass (Tk)	Water vapor (Tf)	Distillation water (Tw)	In	Accommodated	Wasted	
09.00	33.60	39.90	38.00	44.68	42.64				534.60
10.00	35.00	45.40	41.60	52.50	54.02				638.00
11.00	35.40	45.88	43.20	57.20	58.06				635.40
12.00	35.40	45.54	42.60	59.92	63.38				683.00
13.00	35.20	45.54	41.80	60.78	64.04	19.00	1.46	17.25	678.60
14.00	33.20	42.34	40.80	54.86	61.46				409.20
15.00	33.40	40.44	39.40	53.12	57.42				444.20
16.00	32.20	37.64	37.00	48.12	52.06				187.20
Daily	34.18	42.84	40.55	53.90	56.64	19.00	1.46	17.25	526.28

Table 2. Experimental result for stainless steel

Time (hr)	Temperature (^{o}C)				Water (Liter)				Solar intensity (W/m^2)
	Environment (Tl)	Plate (Tp)	Glass (Tk)	Water vapor (Tf)	Distillation water (Tw)	In	Accommodated	Wasted	
09.00	32.80	37.88	33.60	42.24	39.20				587.80
10.00	34.40	40.50	36.00	47.00	46.10				703.00
11.00	35.80	44.92	39.40	53.76	54.86				691.80
12.00	34.20	42.06	39.00	54.12	55.40				587.60
13.00	35.20	43.32	38.00	54.44	55.82	19.00	1.19	17.54	501.80
14.00	34.60	43.46	39.00	52.90	55.68				563.80
15.00	32.60	39.58	36.40	50.60	51.30				574.20
16.00	31.00	36.88	32.40	42.04	44.94				290.60
Daily	33.83	41.08	36.73	49.64	50.41	19.00	1.19	17.54	562.58

Table 3. Experimental result for aluminum

Time (hr)	Temperature (°C)				Water (Liter)				Solar intensity (W/m²)
	Environment (Tl)	Plate (Tp)	Glass (Tk)	Water vapor (Tf)	Distillation water (Tw)	In	Accommodated	Wasted	
09.00	34.80	40.56	37.40	45.82	41.74	19.00	1.48	17.15	679.80
10.00	34.80	44.28	40.00	51.20	51.48				685.20
11.00	35.80	46.06	44.40	57.84	58.86				864.00
12.00	35.40	46.06	45.00	60.52	62.32				725.00
13.00	34.40	42.70	41.40	58.50	61.86				507.80
14.00	34.80	42.84	41.40	58.32	61.76				715.80
15.00	33.80	40.40	38.60	54.14	58.46				709.40
16.00	32.60	37.00	36.40	48.58	52.84				362.80
Daily	34.55	43.49	40.58	54.37	56.17	19.00	1.48	17.15	656.23

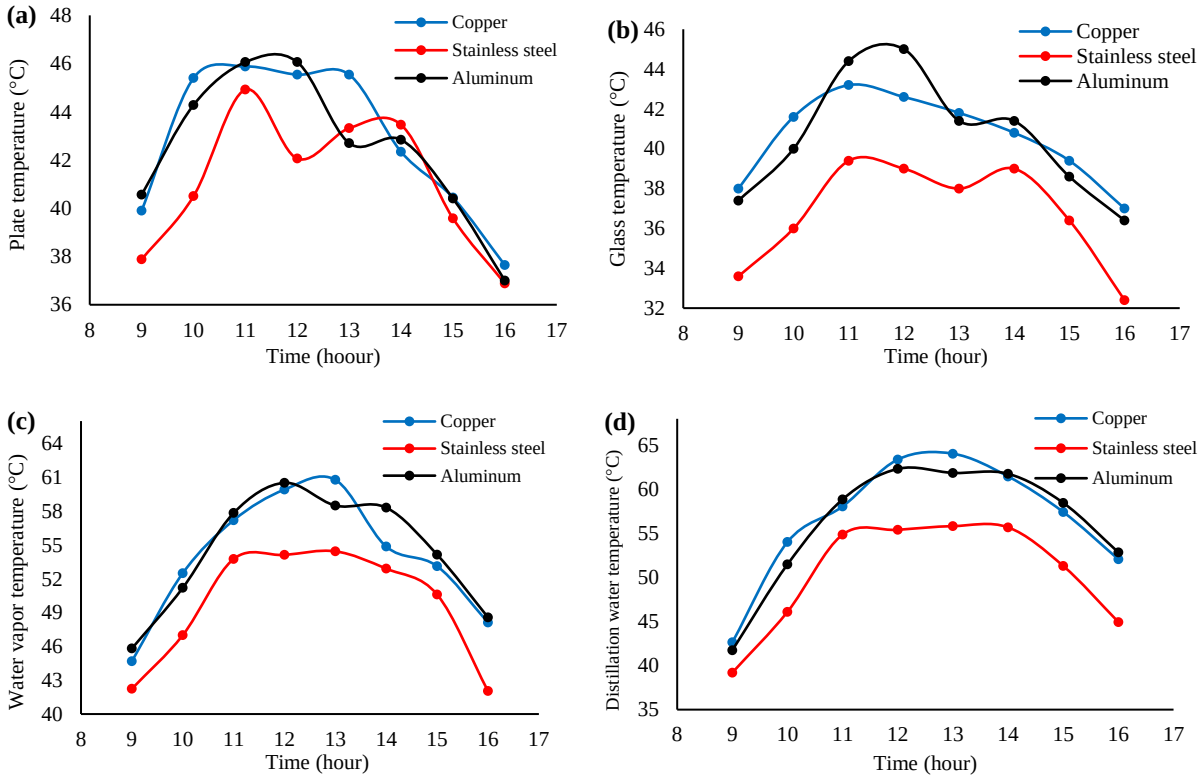

Fig. 6. Solar panel temperature distribution: (a) Plate temperature; (b) Glass temperature; (c) Water vapor temperature; (d) Distillation water temperature

The testing and data collection phases for solar stills composed of copper, stainless steel, and aluminum materials have been concluded. The results indicate that each material exhibits unique characteristics that contribute to the solar still's performance. These results are consistent

with previous studies using the same materials [11], [36]. CFD analysis has been used to investigate the flow pattern and mechanism underlying solar desalination in the solar still. CFD analysis is a reliable research method that is preferred for its cost and time efficiency and its ability to provide detailed phenomena that are not easily obtained through other research methods [34],[35]. The analysis results revealed that each material has a unique flow pattern and mechanism that contributes to the solar still's overall performance. These findings can be used to optimize solar still design and improve their efficiency and effectiveness [39].

Figure 7 illustrates the temperature contour of the solar still for the three material types. The temperature profile is divided into three regions: low, medium, and high-temperature areas. It is observed that the wider the contact space in the solar still, the lower the temperature, and vice versa. This phenomenon is attributed to the entry of solar energy into the solar system through photon particles, which can generate electromagnetic radiation [40]. The area of contact space between photon particles plays a crucial role in their reactivity. The electromagnetic wave spectrum lengthens when the particles have ample space to interact. Conversely, the wavelength shortens when the space is limited and the particles rush. If the distance between particles is extensive, it takes longer for effective collisions to occur, resulting in a slower energy release, which is represented by the blue region. Meanwhile, when the distance between particles is shorter, the release of energy occurs more rapidly, leading to effective collisions marked in red.

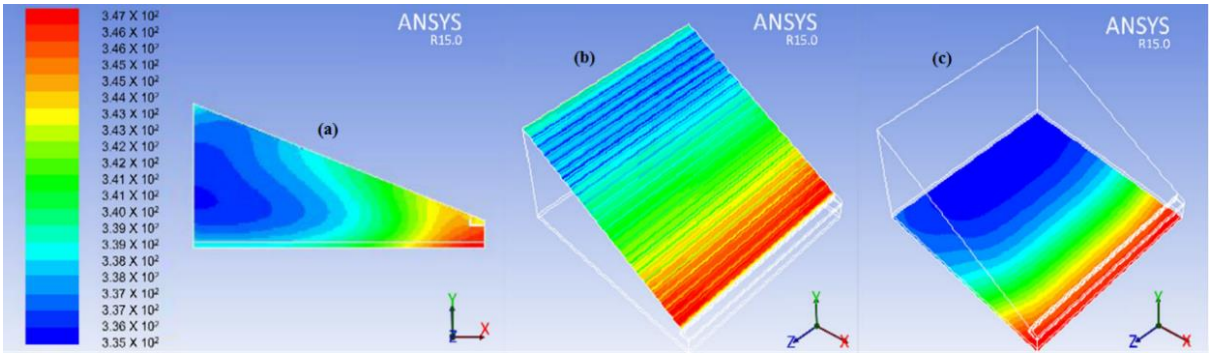

Fig. 7. The temperature contour of solar distillation panel at 1.00 pm. (a) Internal mixture; (b) Glass cover; and (c) Absorbent plate

Upon closer analysis of Figure 7, it is evident that the temperature dynamics display a noticeable increase in the heat transfer coefficient, which indicates a corresponding rise in the Rayleigh number. This trend is due to the variation in contour and color, suggesting a distribution of mass and temperature at the upper and lower ends of the solar stile. This observation is logical and reasonable since the heat transfer coefficient tends to increase as the Rayleigh number increases [41]. Furthermore, Figure 8 provides valuable insights into the water fractions of copper, stainless steel, and aluminum. The simulation results demonstrate that the three materials exhibit distinct water fractions, which can be attributed to the interference and bending of waves around the collector. Specifically, copper appears smoother and calmer, stainless steel exhibits more volatility, while aluminum appears more relaxed. These observations suggest that the materials' surface properties play a crucial role in determining their water fractions.

Additionally, areas marked in red depict high fluctuations, particularly in regions with smaller spaces. This observation suggests that the fluid flow is highly turbulent, which can be attributed to several factors, such as the flow velocity, flow rate, and surface roughness. It is important to note that the high fluctuations can lead to a decrease in the efficiency of the solar collector.

In conclusion, the findings offer valuable insights into the dynamics of temperature and water fractions of various materials, which can aid in the design and development of more efficient and effective solar collectors [42]. It is crucial to consider the surface properties of the materials and the fluid flow dynamics to optimize the collector's performance.

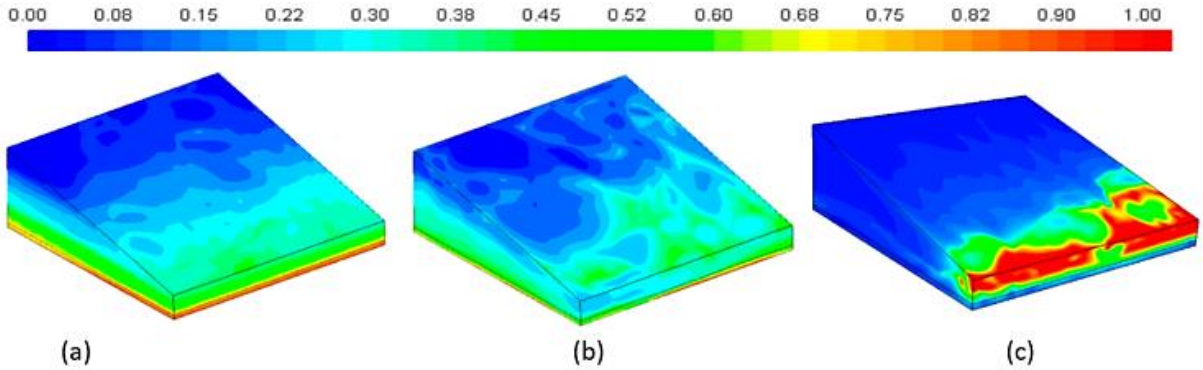

Fig. 8. The water fraction of various materials: (a) Copper; (b) Stainless steel; and (c) Aluminum

Furthermore, the comparison between the experimental and simulation results regarding the amount and productivity of water produced is presented in Figure 9. The results indicate that the collector is highly effective in producing clean water, especially aluminum, with significant similarities observed between the experimental and simulation data. This phenomenon is due to aluminum's effective thermal properties, high specific heat capacity, adjustable reflectance and absorptivity, and corrosion resistance; aluminum swiftly and efficiently heats water and sustains the requisite temperature for optimal evaporation in solar distillation. This analysis is supported by previous research, which simulated the flow of water vapor inside a solar collector [43]. Furthermore, the results clearly demonstrate the considerable impact of installing the proposed partition on various parameters. The partition installation has been proven highly effective in increasing the number of vortices in smaller, thereby prolonging the duration of the heat exchange process and significantly enhancing the still efficiency.

Additionally, the observed rapid temperature changes near the water surface and glass cover provide a clear indication of the occurrence of condensation and evaporation. Overall, these findings suggest that the proposed collector design is effective in producing clean water and has the potential to be further optimized for greater efficiency. Furthermore, the optimization phase at the bottom of the solar still design process is critical, as it involves several essential phenomena that impact the system's efficiency and performance. During this phase, streamlines are a crucial factor, representing the paths taken by fluid particles within the solar still. To ensure that water is evenly distributed across the absorber surface, it is essential to streamline the flow and minimize stagnant zones. This promotes efficient heat transfer and improves steam production [36]. By examining the stream function during bottom optimization,

the solar circulation patterns can still gain insights and make the necessary adjustments to optimize flow dynamics [38]. Isotherms are lines connecting points within the solar system with the same temperature. A uniform temperature distribution should be maintained across the absorber surface during bottom optimization to achieve maximum steam production. This ensures consistent evaporation rates, and by manipulating the layout and design of the bottom section, the distribution of isotherms can be controlled, enhancing heat transfer and improving overall efficiency [23].

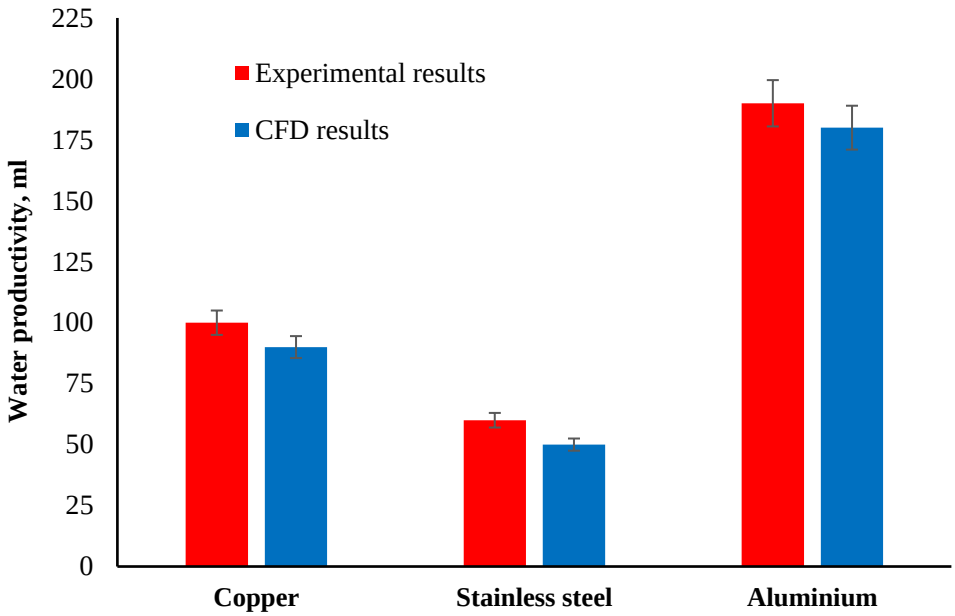

Fig. 9. The comparison of experimental and CFD results of various materials water productivity

Vapor mass fraction is another critical factor to consider during bottom optimization. It refers to the proportion of vapor present in the air-water mixture within the solar still. Optimizing steam production during bottom optimization ensures efficient vapor mass fraction distribution and effective utilization of available heat energy [44]. The effectiveness of a solar still design mainly depends on optimizing the glass cover section. This analysis is very reasonable because shaping the cover material in a well-designed streamline can significantly enhance steam production by influencing several crucial phenomena. Furthermore, the optimization of the glass cover section involves directing the flow of solar radiation toward the absorber surface through the shaping of the cover material. The streamlined cover sections effectively transmit solar energy to the absorber surface and maximize heat input to the system, which ensures efficient solar energy transmission, thus increasing steam production [16]. Moreover, optimizing the glass cover section involves controlling the distribution of temperature gradients. A well-designed isotherm within the cover section helps to maintain a uniform temperature distribution and minimize heat losses, which promotes efficient evaporation and increases steam production. The vapor mass fraction within the glass cover section can also influence steam production by minimizing vapor losses through the cover

material [11]. By optimizing vapor mass fraction distribution, the vapor is efficiently retained within the system, which ultimately enhances steam production.

V. Conclusions

An extensive analysis was conducted to evaluate the effectiveness of three types of solar panels made from different materials. The research found that copper flat plates generated the highest temperature, followed by aluminum, while stainless steel produced the lowest temperature. Additionally, the research noted that convection occurred consecutively in copper flat plates, aluminum, and stainless steel. This observation implies that copper flat plates are more conducive to heat transfer via convection. Furthermore, radiation energy was found to range from highest to lowest for stainless steel flat plates, copper, and aluminum. The highest radiation energy recorded was for stainless steel flat plates, followed by copper and aluminum.

On average, the heat flux recorded across the three materials was approximately 581 W/m^2. This finding indicates that the three materials are somewhat comparable in their heat transfer capabilities. Nonetheless, copper flat plates are more efficient in heat transfer via convection and have the highest temperature, while stainless steel panels have the highest radiation energy. Overall, these findings could inform the development of more efficient solar panels for sustainable energy production.

Acknowledgment

We want to express our gratitude to the Heat Transfer Laboratory of the Mechanical Engineering Department at Jayapura University of Science and Technology for their financial support and provision of materials, test equipment, and measuring instruments, which enabled this research to be completed successfully.

References

[1] M. Nasrollahi, A. Motevali, A. Banakar, and M. Montazeri, "Comparison of the cumulative exergy demand of phase change and reverse osmosis desalination plants with environmental impacts approach," *Desalination*, vol. 572, p. 117156, Mar. 2024, doi: 10.1016/J.DESAL.2023.117156.

[2] H.Y. Nanlohy, H. Riupassa, and M. Setiyo, "Characterizing of Nano Activated Bio-Carbon of Sago Waste as a Homogeneous Combustion Catalyst," *Automot. Exp.*, vol. 7, no. 1, pp. 77–85, Apr. 2024, doi: 10.31603/ae.10619.

[3] A. Sanata, I. Sholahuddin, and H.Y. Nanlohy, "Characterization of biogas as an alternative fuel in micro-scale combustion technology," *Int. J. Integr. Eng.*, vol. 15, no. 4, Aug. 2023, doi: 10.30880/ijie.2023.15.04.006.

[4] V.R. Raju and R.L. Narayana, "Effect of flat plate collectors in series on performance of active solar still for Indian coastal climatic condition," *J. King Saud Univ. - Eng. Sci.*, vol. 30, no. 1, pp. 78–85, Jan. 2018, doi: 10.1016/j.jksues.2015.12.008.

[5] Z. Li, X. Xu, X. Sheng, P. Lin, *et al.*, "Solar-powered sustainable water production: state-of-the-art technologies for sunlight-energy-water nexus," *ACS Nano*, vol. 15, no. 8, pp. 12535–12566, Aug. 2021, doi: 10.1021/ACSNANO.1C01590.

[6] H.Y. Nanlohy, I.N.G. Wardana, M. Yamaguchi, and T. Ueda, "The role of rhodium sulfate

on the bond angles of triglyceride molecules and their effect on the combustion characteristics of crude jatropha oil droplets," *Fuel*, vol. 279, p. 118373, Nov. 2020, doi: 10.1016/j.fuel.2020.118373.

[7] J.U. Kim, S. Lee, S.J. Kang, and T. Il Kim, "Materials and design of nanostructured broadband light absorbers for advanced light-to-heat conversion," *Nanoscale*, vol. 10, no. 46, pp. 21555–21574, Dec. 2018, doi: 10.1039/C8NR06024J.

[8] D. Davra, P. Mehta, N. Patel, and B. Markam, "Solar-enhanced freshwater generation in arid coastal environments: A double basin stepped solar still with vertical wick assistance study in northern Gujarat," *Sol. Energy*, vol. 268, p. 112297, Jan. 2024, doi: 10.1016/J.SOLENER.2023.112297.

[9] M. Gao, L. Zhu, C.K. Peh, and G.W. Ho, "Solar absorber material and system designs for photothermal water vaporization towards clean water and energy production," *Energy Environ. Sci.*, vol. 12, no. 3, pp. 841–864, Mar. 2019, doi: 10.1039/C8EE01146J.

[10] S. Cao, Q. Jiang, X. Wu, D. Ghim, *et al.*, "Advances in solar evaporator materials for freshwater generation," *J. Mater. Chem. A*, vol. 7, no. 42, pp. 24092–24123, 2019, doi: 10.1039/C9TA06034K.

[11] S. Tian, X. Li, J. Ren, Z. Zhou, *et al.*, "Emerging heat-localized solar distillation systems: Solar interfacial distillation VS photothermal membrane distillation," *Desalination*, vol. 572, p. 117147, Mar. 2024, doi: 10.1016/J.DESAL.2023.117147.

[12] X. Liu, D. D. Mishra, X. Wang, H. Peng, and C. Hu, "Towards highly efficient solar-driven interfacial evaporation for desalination," *J. Mater. Chem. A*, vol. 8, no. 35, pp. 17907–17937, Sep. 2020, doi: 10.1039/C9TA12612K.

[13] Z. Xu, Z. Li, Y. Jiang, G. Xu, *et al.*, "Recent advances in solar-driven evaporation systems," *J. Mater. Chem. A*, vol. 8, no. 48, pp. 25571–25600, Dec. 2020, doi: 10.1039/D0TA08869B.

[14] Z. Zhao, C. Wang, D. Wei, and F. Wang, "Condensation device design represents a critical step for solar-driven water evaporation toward practical applications," *Cell Rep. Phys. Sci.*, vol. 5, no. 2, p. 101794, Feb. 2024, doi: 10.1016/J.XCRP.2024.101794.

[15] V. Kashyap and H. Ghasemi, "Solar heat localization: Concept and emerging applications," *J. Mater. Chem. A*, vol. 8, no. 15, pp. 7035–7065, Apr. 2020, doi: 10.1039/D0TA01004A.

[16] T. Yan, G. Xie, H. Liu, Z. Wu, and L. Sun, "CFD investigation of vapor transportation in a tubular solar still operating under vacuum," *Int. J. Heat Mass Transf.*, vol. 156, p. 119917, Aug. 2020, doi: 10.1016/J.IJHEATMASSTRANSFER.2020.119917.

[17] M.R. Salem, R.Y. Sakr, G.M.R. Assassa, and O.A. Aly, "Augmentation of solar still distillation performance using waste heat energy and guiding vanes: A field study," *Desalination*, vol. 572, p. 117150, Mar. 2024, doi: 10.1016/J.DESAL.2023.117150.

[18] X. Zhou, F. Zhao, P. Zhang, and G. Yu, "Solar water evaporation toward water purification and beyond," *ACS Mater. Lett.*, vol. 3, no. 8, pp. 1112–1129, Aug. 2021, doi: 10.1021/ACSMATERIALSLETT.1C00304.

[19] L. Zhang, Z. Xu, L. Zhao, B. Bhatia, *et al.*, "Passive, high-efficiency thermally-localized solar desalination," *Energy Environ. Sci.*, vol. 14, no. 4, pp. 1771–1793, Apr. 2021, doi: 10.1039/D0EE03991H.

[20] J. Huang, H. Zheng, and H. Kong, "Key pathways for efficient solar thermal desalination," *Energy Convers. Manag.*, vol. 299, p. 117806, Jan. 2024, doi:

10.1016/J.ENCONMAN.2023.117806.
[21] F. He, X. Wu, J. Gao, and Z. Wang, "Solar-driven interfacial evaporation toward clean water production: burgeoning materials, concepts and technologies," *J. Mater. Chem. A*, vol. 9, no. 48, pp. 27121–27139, Dec. 2021, doi: 10.1039/D1TA08886F.
[22] Z. Zhu, Y. Xu, Y. Luo, W. Wang, and X. Chen, "Porous evaporators with special wettability for low-grade heat-driven water desalination," *J. Mater. Chem. A*, vol. 9, no. 2, pp. 702–726, Jan. 2021, doi: 10.1039/D0TA09193F.
[23] H. Ben Bacha, A.S. Abdullah, Z.M. Omara, and F.A. Essa, "Enhancing freshwater production in solar distillation: Hemispherical absorber modification and reflectors integration," *Sustain. Energy Technol. Assess.*, vol. 61, p. 103576, Jan. 2024, doi: 10.1016/J.SETA.2023.103576.
[24] K. El Kadi, I. Adeyemi, and I. Janajreh, "Application of directional freezing for seawater desalination: Parametric analysis using experimental and computational methods," *Desalination*, vol. 520, p. 115339, Dec. 2021, doi: 10.1016/J.DESAL.2021.115339.
[25] A. Atiz, M. Erden, and M. Karakilcik, "Hydrogen production of flat plate solar collectors integrated with photovoltaic thermal panels," *Int. J. Hydrog. Energy*, vol. 52, pp. 1408–1424, Jan. 2024, doi: 10.1016/j.ijhydene.2023.08.302.
[26] A.S. Jawed, L. Nassar, H.M. Hegab, F.A. Marzooqi, *et al.*, "Recent developments in solar-powered membrane distillation for sustainable desalination," *Heliyon*, vol. 10, no. 11, p. e31656, Jun. 2024, doi: 10.1016/j.heliyon.2024.e31656.
[27] A.Q. Al-Dujaili, A.H. Shallal, A.H. Sabry, O.I. Dallal Bashi, Y.M. Alkubaisi, and A.J. Humaidi, "Maximizing solar energy utilization and controlling electrical consumption in domestic water heaters by integrating with aluminum reflector," *Measurement*, vol. 230, p. 114558, May 2024, doi: 10.1016/j.measurement.2024.114558.
[28] M. El Hadi Attia, A.E. Kabeel, M. Abdelgaied, A. Aljabri, and M.A. Elazab, "Performance optimization and comparative study of a conical solar distiller with optimized construction of aluminium balls as energy storage materials," *Desalination Water Treat.*, vol. 319, p. 100504, Jul. 2024, doi: 10.1016/j.dwt.2024.100504.
[29] J. Mustafa, M.M. Abdullah, S. Husain, S. Alqaed, E.H. Malekshah, and M. Sharifpur, "A two-phase analysis of the use of water-aluminum nanofluid in a solar still with a layer of phase change materials," *Eng. Anal. Bound. Elem.*, vol. 152, pp. 627–636, Jul. 2023, doi: 10.1016/j.enganabound.2023.04.030.
[30] A. Sajedi, S.D. Farahani, and A. Alizadeh, "Numerical investigation and group method of data handling -based prediction on new flat plate solar collector integrated with nanoparticles enhanced phase change materials and tube rotation mechanism," *J. Energy Storage*, vol. 67, p. 107542, Sep. 2023, doi: 10.1016/j.est.2023.107542.
[31] A. Ansari, F.M. Galogahi, G. Millar, F. Helfer, *et al.*, "Computational fluid dynamics simulations of solar-assisted, spacer-filled direct contact membrane distillation: Seeking performance improvement," *Desalination*, vol. 545, p. 116181, Jan. 2023, doi: 10.1016/j.desal.2022.116181.
[32] M. Mohammadi, S. Vakilipour, and R. Hekmatkhah, "Unsteady film condensation underneath the inclined wall of a solar still desalination system," *Int. Commun. Heat Mass Transf.*, vol. 156, p. 107632, Aug. 2024, doi: 10.1016/j.icheatmasstransfer.2024.107632.
[33] P.I. Babb, S.F. Ahmadi, F. Brent, R. Gans, *et al.*, "Salt-rejecting continuous passive solar thermal desalination via convective flow and thin-film condensation," *Cell Rep. Phys. Sci.*,

vol. 4, no. 12, p. 101682, Dec. 2023, doi: 10.1016/j.xcrp.2023.101682.
[34] S. Saha, M.R.I. Sarker, M.A. Kader, M.M. Ahmed, S.S. Tuly, and N.N. Mustafi, "Development of a vacuum double-slope solar still for enhanced freshwater productivity," *Sol. Energy*, vol. 270, p. 112385, Mar. 2024, doi: 10.1016/J.SOLENER.2024.112385.
[35] M.U. Farid, J.A. Kharraz, S. Sharma, R.J. Khan, *et al.*, "Technological advancements in water heating approaches for membrane distillation desalination process: From bulk to localized heating," *Desalination*, vol. 574, p. 117235, Apr. 2024, doi: 10.1016/J.DESAL.2023.117235.
[36] M. Tawalbeh, S. Mohammed, A. Alnaqbi, S. Alshehhi, and A. Al-Othman, "Analysis for hybrid photovoltaic/solar chimney seawater desalination plant: A CFD simulation in Sharjah, United Arab Emirates," *Renew. Energy*, vol. 202, pp. 667–685, Jan. 2023, doi: 10.1016/J.RENENE.2022.11.106.
[37] N. Prakash, A. Chaudhuri, and S.P. Das, "Numerical modelling and analysis of concentration polarization and scaling of gypsum over RO membrane during seawater desalination," *Chem. Eng. Res. Des.*, vol. 190, pp. 497–507, Feb. 2023, doi: 10.1016/J.CHERD.2022.12.050.
[38] S. Shoeibi, H. Kargarsharifabad, N. Rahbar, G. Ahmadi, and M.R. Safaei, "Performance evaluation of a solar still using hybrid nanofluid glass cooling-CFD simulation and environmental analysis," *Sustain. Energy Technol. Assess.*, vol. 49, no. November 2021, p. 101728, 2022, doi: 10.1016/j.seta.2021.101728.
[39] W. Sun, Z. Liu, Y. Liu, and Z. Wang, "Enhancing freshwater production with a high-performance solar interface evaporator and in low-vacuum environment: A solar-driven low-vacuum interfacial distillation system," *Desalination*, vol. 568, p. 117014, Dec. 2023, doi: 10.1016/J.DESAL.2023.117014.
[40] Y. Elhenawy, M. Bassyouni, K. Fouad, A.M. Sandid, M.A.E.R. Abu-Zeid, and T. Majozi, "Experimental and numerical simulation of solar membrane distillation and humidification – dehumidification water desalination system," *Renew. Energy*, vol. 215, p. 118915, Oct. 2023, doi: 10.1016/J.RENENE.2023.118915.
[41] A.A.V. Lisboa, R. Segurado, and M.A.A. Mendes, "Solar still performance for small-scale and low-cost seawater desalination: Model-based analysis and water yield enhancement techniques," *Sol. Energy*, vol. 238, pp. 341–362, May 2022, doi: 10.1016/J.SOLENER.2022.04.007.
[42] F. Lou, S. Nie, F. Yin, W. Lu, *et al.*, "Numerical and experimental research on the integrated energy recovery and pressure boost device for seawater reverse osmosis desalination system," *Desalination*, vol. 523, p. 115408, Feb. 2022, doi: 10.1016/J.DESAL.2021.115408.
[43] S.S. Al Saleem, E. Al-Qadami, H.Z. Korany, Md. Shafiquzzaman *et al.*, "Computational fluid dynamic applications for solar stills efficiency assessment: A review," *Sustain. Switz.*, vol. 14, no. 17, 2022, doi: 10.3390/su141710700.
[44] O. Prakash, A. Ahmad, A. Kumar, S.M. Mozammil Hasnain, and G. Kumar, "Comprehensive analysis of design software application in solar distillation units," *Mater. Sci. Energy Technol.*, vol. 5, pp. 171–180, Jan. 2022, doi: 10.1016/j.mset.2022.01.005.